

## Atmospheric Predictability of Seasonal, Annual, and Decadal Climate Means and the Role of the ENSO Cycle: A Model Study

WILBUR Y. CHEN AND HUUG M. VAN DEN DOOL

*Climate Prediction Center, NOAA/NWS/NCEP, Washington, D.C.*

(Manuscript received 21 March 1996, in final form 30 August 1996)

### ABSTRACT

The characteristics of extratropical low-frequency variability are examined using a comprehensive atmospheric general circulation model. A large experiment consisting of 13 45-yr-long integrations forced by prescribed sea surface temperature (SST) variations is analyzed. The predictability of timescales of seasonal to decadal averages is evaluated. The variability of a climate mean contains not only climate signal arising from external boundary forcing but also climate noise due to the internal dynamics of the climate system, resulting in various levels of predictability that are dependent on the forcing boundary conditions and averaging timescales. The focus of this study deviates from the classic predictability study of Lorenz, which is essentially initial condition sensitive. This study can be considered to be a model counterpart of Madden's "potential" predictability study.

The tropical SST anomalies impact more on the predictability over the Pacific/North America sector than the Atlantic/Eurasia sector. In the former sector, more significant and positive impacts are found during El Niño and La Niña phases of the ENSO cycle than during the ENSO inactive period of time. Furthermore, the predictability is significantly higher during El Niño than La Niña phases of the ENSO cycle. The predictability of seasonal means exhibits large seasonality for both warm and cold phases of the ENSO cycle. During the warm phases, a high level of predictability is observed from December to April. During the cool phases, the predictability rapidly drops to below normal from November to March. The spring barrier in the atmospheric predictability is therefore a distinct phenomenon for the cold phase, not the warm phase, of the ENSO cycle. The cause of the barrier can be traced to the smaller climate signal and larger climate noise generated during cold events, which in turn can be traced back to the rapidly weakening negative SST anomalies in the tropical Pacific east of the date line.

Due to the fact that the signal to noise ratio of this model climate system is very small, an upper bound in atmospheric predictability is present, even when a perfect model atmosphere is considered and large ensemble mean predictions are exploited. The outstanding issues of the dynamical short-term climate prediction employing an atmospheric general circulation model are examined, the current model deficiencies identified, and continuing efforts in model development addressed.

### 1. Introduction

The atmospheric predictability of a climate mean at timescales of a season or longer is examined employing a comprehensive atmospheric general circulation model (AGCM). An approach and emphasis different from the classical predictability study of Lorenz (1982) are adopted here and the results and implications discussed. The classical studies focus on growth rate of an initial error (Lorenz 1965; Smagorinsky 1969; Shukla 1981) and determine the limit to the deterministic predictability, which has been established to be about 3 weeks for an instantaneous atmospheric state (e.g., Lorenz 1982; Dalcher and Kalnay 1987; Roads 1987; Palmer and Tibaldi 1988; Schubert and Suarez 1989; Tracton et al.

1989; Chen 1989; Van den Dool 1994). Some potential predictability beyond this limit has also been demonstrated for time means (or lower-frequency variations) (e.g., Shukla 1981; Blackmon et al. 1983; Miyakoda et al. 1986; Mansfield 1986; Roads 1986). The initial error divergence approach has also been explored in the El Niño–Southern Oscillation (ENSO; Rasmusson and Wallace 1983) associated predictability studies (Fraedrich 1988; Goswami and Shukla 1991; Blumenthal 1991).

Although covering a wide range of timescales, from instantaneous state to interannual variability, the classic predictability studies have one thing in common: they examine the loss of predictability due to growth and divergence of an initial error. The classic study is therefore on the predictability that is initial condition sensitive (ICS).

In this article, we will look into the predictability that is boundary condition dependent (BCD). After (and before) complete loss of the ICS predictability, the atmosphere might possess BCD predictability due to the

---

*Corresponding author address:* Dr. Wilbur Chen, Climate Prediction Center, National Centers for Environmental Prediction, 5200 Auth Rd., Camp Springs, MD 20233.  
E-mail: wd51wc@sun1.wvv.noaa.gov

existence of externally forced variability. There are situations when (or where) the predictability is both initial and boundary condition dependent. For our present study, we will focus on those that are only boundary value dependent. For a pair of 45-yr-long AGCM runs forced by identical, prescribed time varying boundary conditions, it is easy to comprehend that the initial conditions will become irrelevant after some time. After this initial condition sensitive period, the predictability evaluated from the similarity of anomalies in the pair occurring at the same time can exhibit varying magnitude depending on the underlying forcing boundary conditions. We will explore this kind of boundary-condition-dependent predictability, for climate means ranging from seasonal, annual, to decadal timescales, for the northern extratropical atmosphere.

The interannual variability of a climate mean consists of not only climate signal but also climate noise. The climate signals are those variations forced by the slowly varying anomalous boundary conditions external to the climate system (e.g., Hoskins and Karoly 1981; Horel and Wallace 1981; Wallace and Blackmon 1983; Blackmon et al. 1983; Cubash 1985), while the climate noise is due to the dynamical nature internal to a fluid flow even when the external forcing is constant (e.g., Leith 1973; Jones 1975; Madden 1976; Lau 1981; Trenberth 1984; Chervin 1986; Zwiers 1987; Chen and Van den Dool 1995a). The climate noise, as the words imply, can not be predicted beyond some point, generally believed to be about 3 weeks. However, a climate anomaly may display a certain degree of predictability if the percentage of climate signal in its total variability is large enough to overcome the destructive effect of the climate noise.

In the real world, it is exceedingly difficult to separate climate signal from climate noise (Trenberth 1984; Chervin 1986; Zwiers 1987). For the GCM climate variability simulations, the signal to noise separation problem becomes manageable. Approaches and formulism to separate signal from noise and the analysis of the interannual variability in an ensemble of climate simulations can be found in Folland and Rowell (1995) and Zwiers (1996). In this article, we are interested in what level of boundary condition dependent predictability the extratropical atmosphere displays. Is there a large difference in this kind of predictability over the Pacific/North America (PNA) sector from the Atlantic/Eurasia (AEA) sector? Are there substantial differences in the level of BCD predictability during El Niño, La Niña, and ENSO inactive years? Furthermore, is there also a "spring barrier" in the BCD predictability in the extratropical atmosphere? If there is a spring barrier, can we gain some insights into the physical processes?

## 2. Data and treatments

The ocean-atmosphere coupled model group of the National Centers for Environmental Predictions (NCEP) has conducted a large climate variability experiment in

1995 (M. Ji 1996, personal communication). Altogether, 13 45-year-long AGCM runs have been generated at a reduced resolutions of T40L18 by a global spectral model developed for medium-range forecasting (MRF) at NCEP. A complete documentation of the MRF system can be found in Sela (1980), with updates of the model by Kanamitsu (1989), Kalnay et al. (1990), and Kumar et al. (1996). All 13 runs began in January 1950 and integrated out to 45 years ending in February 1995. The sea surface temperatures were prescribed for the entire 45 years using NCEP's SST analyses. That is, the model was run in perfect ocean uncoupled mode. For the early period when no operational SST analyses were available, the NCEP's "reanalysis" for the period 1950–92 (T. M. Smith et al. 1997, manuscript submitted to *J. Climate*) was used. The solar radiation was updated every day according to the astronomical calendar. The snow depth, soil moisture, and sea ice conditions were updated every day according to their known climatologies. The Hadley Centre of the U.K. Meteorological Office has made a similar but less restricted ensemble of multidecadal AGCM integrations (Folland and Rowell 1995), forced by not only the observed SST but also the observed sea ice data. The snow, ice, and surface hydrology may be important components of the mechanisms that induce the climate's remote response to the slow SST variations. Our current study cannot reflect this possible response due to the use of climatological snow, ice-cover data.

In this study, the geopotential height fields at 500-mb level (Z500) were employed. The climatologies for each month were constructed first by averaging that month over all 45 years and over all 13 runs. A set of monthly anomalies was then obtained by subtracting the climatology from the monthly data. Since the seasonal to decadal timescale predictability is to be evaluated, we form the seasonal, yearly, and decadal means (denoted by SM, YM, and DM, respectively) first in the following manner. Let  $\text{anom}(m, i, k)$  stand for an anomaly for month ( $m$ ), year ( $i$ ), and AGCM run number ( $k$ ). Then we form

SM( $m, i, k$ ) by averaging  $\text{anom}(m, i, k)$  over 3 months centered on  $m$ ;

YM( $i, k$ ) by averaging  $\text{anom}(m, i, k)$  over all  $m$  from August of year ( $i - 1$ ) to July of year  $i$ ; and

DM( $l, k$ ) by averaging YM( $i, k$ ) over 10 years, where

$l = 1$  for 1951–60,

$l = 2$  for 1961–70,

$l = 3$  for 1971–80, and

$l = 4$  for 1981–90.

Note that the anomaly and the averaged SM, YM, and DM all are a function of position.

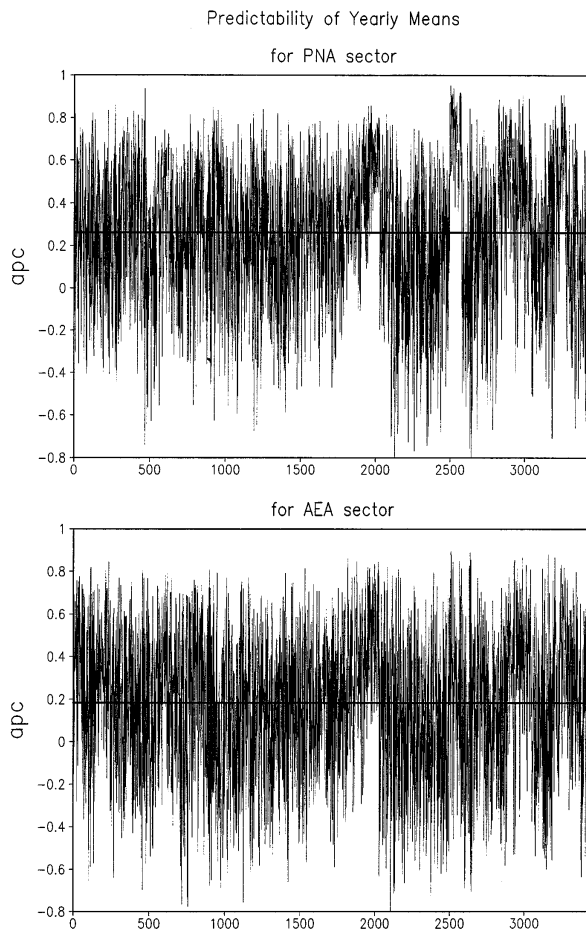


FIG. 1. The mean (horizontal bold line) and fluctuations of the yearly mean predictability, measured by anomaly pattern correlation. The x axis shows the case number of a total of  $78 \times 44 (=3432)$  cases. Spatial domains are the PNA sector for  $120^\circ\text{E}$  eastward to  $60^\circ\text{W}$  and the AEA sector for  $60^\circ\text{W}$  eastward to  $120^\circ\text{E}$ . Both domains cover only from  $20^\circ$  to  $70^\circ\text{N}$ .

We choose the anomaly pattern correlation (APC) as a measure to gauge the level of predictability that we are interested in. Between a pair of anomaly fields, denoted here by  $a$  and  $b$ , APC is defined as in Miyakoda (1972) and Saha and Van den Dool (1988):

$$\text{APC} = \frac{[ab]}{[a^2]^{1/2}[b^2]^{1/2}}, \quad (1)$$

where the  $[\ ]$  represents averaging over the spatial domain of interest. In addition to hemispheric averaging (NH), which covers the area from  $20^\circ\text{N}$  to  $70^\circ\text{N}$ , two smaller longitudinal domains are also considered: one is over the North Pacific/North America sector ( $120^\circ\text{E}$  eastward to  $60^\circ\text{W}$ ) and the other the North Atlantic/Eurasia sector ( $60^\circ\text{W}$  eastward to  $120^\circ\text{E}$ ).

Note that a collection of APCs can be obtained for each year for SMs and YMs by correlating all possible pairs valid at the same time. With 13 runs that provide

TABLE 1. Mean (M) and standard deviation (SD) of APCs before and after the Fisher's Z transformation for yearly and decadal climate means.

| Time-scale | Z trans-formation | Northern Hemisphere |      | PNA sector |      | AEA sector |      |
|------------|-------------------|---------------------|------|------------|------|------------|------|
|            |                   | M                   | SD   | M          | SD   | M          | SD   |
| Yearly     | Before            | 0.22                | 0.28 | 0.26       | 0.34 | 0.18       | 0.33 |
|            | After             | 0.25                | 0.33 | 0.31       | 0.41 | 0.21       | 0.39 |
| Decadal    | Before            | 0.40                | 0.27 | 0.45       | 0.25 | 0.34       | 0.35 |
|            | After             | 0.46                | 0.33 | 0.54       | 0.33 | 0.41       | 0.43 |

altogether 78 APCs each year, we are thus able to obtain a statistically stable estimate of APC as follows:

$$\text{APC} = \frac{1}{44 \times 78} \sum_{i=1}^{44} \sum_{j=1}^{78} \text{APC}_{ij}. \quad (2)$$

Note that there are only 44 YMs (as defined previously by averaging from August to the following July) although there are 45 years of the monthly data. For DMs the number is 4 instead of 44.

### 3. Predictability of the seasonal to decadal means

The seasonal to decadal climate mean predictability is estimated by the above formula. Based on a perfect model point of view, each run represents a sample of the true model atmospheric states, thus serving as a prediction for any other run as well as being a realization to be verified against. An APC can therefore be obtained between any pair among the 13 realizations to represent a sampled "skill score." Note that the observed atmospheric states are not invoked and verified with; the APC thus obtained is only an idealistic, henceforth a theoretical or potential predictability, not a practical or easily realizable skill level.

Figure 1 presents the mean and the fluctuations of the boundary condition dependent predictability for the yearly means. The x axis shows the case number of a total of  $78 \times 44 (=3432)$  cases. The horizontal bold line represents the mean of the 3432 APCs. The upper panel is the results for the PNA sector, and the lower panel is for the AEA sector. The means and standard deviations are listed in Table 1 along with some statistical significance data to be discussed shortly. We see that both mean predictability levels are small, less than 0.26. However, the mean (APC) for the PNA sector is noticeably larger than that for the AEA sector, implying that larger (or better detectable) impact of the SST forcing can be found in the PNA than in the AEA sector.

The APC difference between PNA and AEA sectors appears to be small, 0.26 versus 0.18, especially when considering the large standard deviations associated with both of them. Is the difference between these two means statistically significant? We proceed to make a statistical significance test.

The probability distribution of the APCs reported here

is not Gaussian but highly skewed. This is because the APCs are bounded by +1 (and -1). Branstator (1986) has examined the problem pertaining to the interpretation of variability from two time periods. A simple Fisher's Z transformation (e.g., Morrison 1983) on APCs, that is,

$$Z(\text{APC}) = \frac{1}{2} \ln\left(\frac{1 + \text{APC}}{1 - \text{APC}}\right), \quad (3)$$

will make the new distribution more Gaussian and comparison of variability in Z distribution will be more meaningful. For this reason, we obtained Z(APC) and list their means and standard deviations also in Table 1.

Now, let us form a null hypothesis that there is no real difference between the two means. Let  $\mu$  and  $\sigma$  stand for mean and standard deviation, in general, and  $X_1$  and  $X_2$  the sample means obtained in large samples of size  $N_1$  and  $N_2$ , drawn from respective populations having means  $\mu_1$  and  $\mu_2$  and standard deviations  $\sigma_1$  and  $\sigma_2$ . Since a null hypothesis is assumed, we should have

$$\mu_{(X_1 - X_2)} = \mu_{X_1} - \mu_{X_2} = \mu_1 - \mu_2 = 0. \quad (4)$$

According to sampling theory (e.g., Morrison 1983), we should also have

$$\sigma_{(X_1 - X_2)} = (\sigma_1^2/N_1 + \sigma_2^2/N_2)^{1/2}. \quad (5)$$

Next, let us standardize the difference variable ( $X_1 - X_2$ ) to obtain the z score by

$$\begin{aligned} z &= \frac{(X_1 - X_2) - \mu_{(X_1 - X_2)}}{\sigma_{(X_1 - X_2)}} \\ &= \frac{(X_1 - X_2)}{(\sigma_1^2/N_1 + \sigma_2^2/N_2)^{1/2}}. \end{aligned} \quad (6)$$

Using the sample standard deviations (those listed in Table 1) as estimates of  $\sigma_1$  and  $\sigma_2$ , we can now test the null hypothesis at any level of significance. Now, we have

$$z = \frac{0.31 - 0.21}{(0.41^2/3432 + 0.39^2/3432)^{1/2}} = 10.0.$$

With a critical value  $z_c = 10.0$ , a Gaussian distribution table assures us that the null hypothesis can be true with probability of near zero. Therefore, the APC difference between PNA and AEA sectors (0.26 vs 0.18) is statistically significant at a confidence level of 100%. We are thus as sure as can be that the tropical SST anomalous forcing impacts more over the PNA sector than the AEA sector in the northern extratropical atmosphere in this model.

The decadal-mean predictability (Fig. 2) shows much larger APCs than those of the yearly means and pronounced variability from one decade to the next. The x axis is again the case number of a total of  $78 \times 4 (=312)$  cases. The larger decadal APC than the yearly APC is expected since the model climate noise of a decadal mean is much smaller than that of the yearly mean, and it is understood that the noise always degrades an APC.

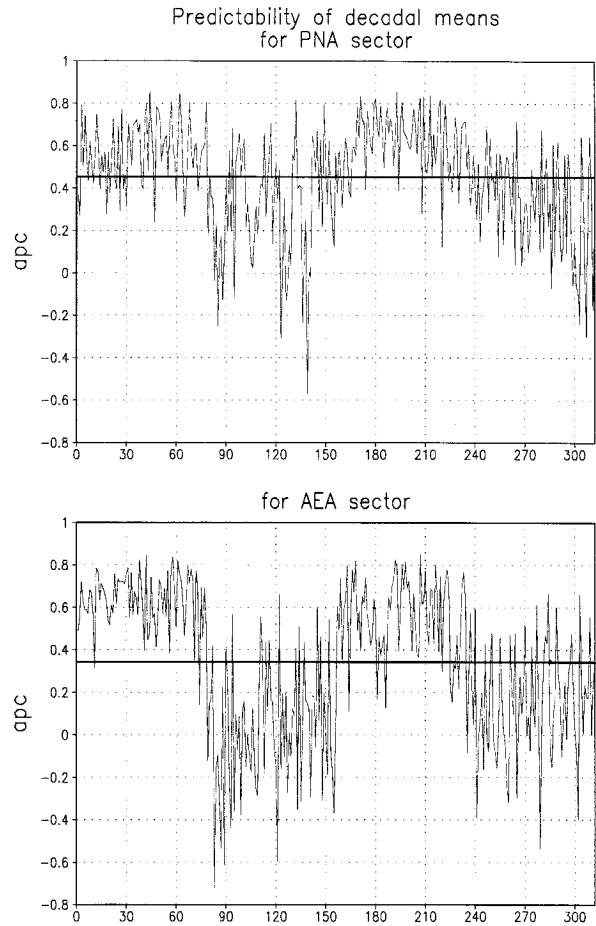


FIG. 2. As in Fig. 1 except for the decadal-mean predictability instead of the yearly mean. The x axis shows the case number of a total of  $78 \times 4 (=312)$  cases.

The statistics of the decadal predictability are also listed in Table 1. The APC difference between PNA and AEA sectors, 0.54 versus 0.41, is again statistically significant. The decadal  $z_c$ , between PNA and AEA sectors, obtained by Eq. (6) is 4.05. It is not as large as that of the yearly  $z_c$  mainly because of the much smaller sample size, 3432 versus 312. However, the Gaussian table assures us that the difference in the decadal APC between PNA and AEA sectors is statistically significant with a confidence level of 100%.

Another interesting feature observed in Fig. 2 is the large variability in the mean predictability from one decade to the next, especially so for the AEA sector. Note that there are 4 decades of APC in the figure, with 78 pairs for each decade. The statistics of each 78-pair subgroup (decade) are listed in Table 2. Taking AEA sector for example, the mean predictability drops from 0.63 to 0.02 from the 1951-60 decade to the 1961-70 decade; then it rises to 0.56 for the 1971-80 decade and then drops back down again to 0.15 for the 1981-90 decade. For this case, the change in mean predictability

TABLE 2. Mean (M) and standard deviation (SD) of APCs before and after Fisher's Z transformation for decadal climate means of all 4 decades.

| Decade  | Z trans-formation | Northern Hemisphere |      | PNA sector |      | AEA sector |      |
|---------|-------------------|---------------------|------|------------|------|------------|------|
|         |                   | M                   | SD   | M          | SD   | M          | SD   |
| 1951–60 | Before            | 0.60                | 0.11 | 0.57       | 0.16 | 0.63       | 0.13 |
|         | After             | 0.71                | 0.18 | 0.68       | 0.25 | 0.78       | 0.22 |
| 1961–70 | Before            | 0.16                | 0.25 | 0.31       | 0.28 | 0.02       | 0.30 |
|         | After             | 0.17                | 0.27 | 0.34       | 0.33 | 0.02       | 0.34 |
| 1971–80 | Before            | 0.59                | 0.13 | 0.62       | 0.15 | 0.56       | 0.18 |
|         | After             | 0.70                | 0.21 | 0.76       | 0.25 | 0.68       | 0.28 |
| 1981–90 | Before            | 0.25                | 0.19 | 0.32       | 0.23 | 0.15       | 0.26 |
|         | After             | 0.26                | 0.21 | 0.36       | 0.27 | 0.17       | 0.29 |

from one decade to the next is statistically significant according to the  $z$  statistics and Eq. (6).

It should be interesting to explore why the 1950s and 1970s have much higher predictability than the other two decades. But, this effort will diffuse our current focus. We will try to expand on this interesting subject elsewhere.

The roles the climate signal and climate noise play in determining the boundary condition dependent predictability will be discussed in detail in the next section. The seasonal means were constructed for all 12 overlapping seasons (December–February (DJF), January–March, and February–April, etc.). The seasonality of the seasonal-mean predictability can be detected if there is any. The characteristics will be discussed in later sections in detail.

#### 4. Variance of climate signal and climate noise

In order to account for the higher level of predictability for the PNA sector than the AEA sector and why the decadal-mean predictability is larger than the yearly mean predictability, we resort to the geographical distributions of the climate signal and noise of this model climate variability. In a recent workshop on simulations of the climate of the twentieth century held at the Hadley Centre, Rowell (1995) presented a methodology for using an ensemble of multidecadal GCM simulations to assess the percentage variance explained by SST forcing. Zwiers (1996) has also described a formalism for analyzing the interannual variability and predictability in an ensemble of climate simulations. For our present purpose of assessing the boundary condition dependent predictability, the Rowell's methodology appears to be suitable. We therefore follow Rowell to define our model climate signal and noise.

For illustrative purposes, we use the yearly means. At a given location, let a yearly mean anomaly be denoted by  $a_{ik}$ , where  $i$  is the year index that goes from 1 to 44 and  $k$  the case number of the AGCM run that goes from 1 to 13. For year  $i$ , the climate signal ( $CS_i$ ) is estimated as the average of all 13 cases, that is,

$$CS_i = \frac{1}{13} \sum_{k=1}^{13} a_{ik}. \quad (7)$$

The climate noise for run number  $k$  and year  $i$  ( $CN_{ik}$ ) is simply a deviation from the signal, that is,

$$CN_{ik} = a_{ik} - CS_i. \quad (8)$$

The variance of the model climate noise for year  $i$  ( $vn_i$ ) can then be obtained by

$$vn_i = \frac{1}{(13 - 1)} \sum_{k=1}^{13} CN_{ik}^2. \quad (9)$$

Note that the denominator is 12 instead of 13 because the degrees of freedom are one less than the total number of realizations for a second moment.

Let VN represent the average of noise variance over 44 years; then,

$$VN = \frac{1}{44} \sum_{i=1}^{44} vn_i. \quad (10)$$

Although the monthly mean climatology is already removed from the monthly dataset, we recalculate the yearly mean climatology as

$$\text{clim} = \frac{1}{44} \sum_{i=1}^{44} CS_i. \quad (11)$$

The variance of the climate signal (VS) is simply obtained with reference to the clim, as

$$VS = \frac{1}{(44 - 1)} \sum_{i=1}^{44} (CS_i - \text{clim})^2. \quad (12)$$

Again, there is one less than the total degrees of freedom for this second moment.

In Eq. (7), the climate signal for a given year is obtained from an ensemble of only 13 members. It represents a small sample estimate, albeit a fairly good one. Because of the uncertainty in  $CS_i$  from the true population climate signal, the VS obtained by Eq. (12) will always overestimate the externally forced international variability. The amount of overestimation is  $VN/13$ , according to a standard analysis of variance (e.g., Scheffe 1959, 226). For our current interest in understanding the qualitative aspect of the boundary condition dependent predictability, Eq. (12) is probably good enough.

Figure 3 presents the variance of the yearly mean climate signal and noise for Z500 (the unit is  $m^2$ ). The climate noise variance is, in general, considerably larger than the variance of the signal. The signal develops mainly over the North Pacific, between Hawaii and the Aleutian Islands. A lesser amount of signal variance is found over western Canada and the Arctic Siberia. A large amount of climate noise develops over the Arctic Siberia, where the noise variance is overwhelming when compared with the noise variance over the northeastern Pacific, explaining why the APC for the AEA sector is significantly smaller than that of the PNA sector. Over the North Pacific sector, it is interesting to note that the

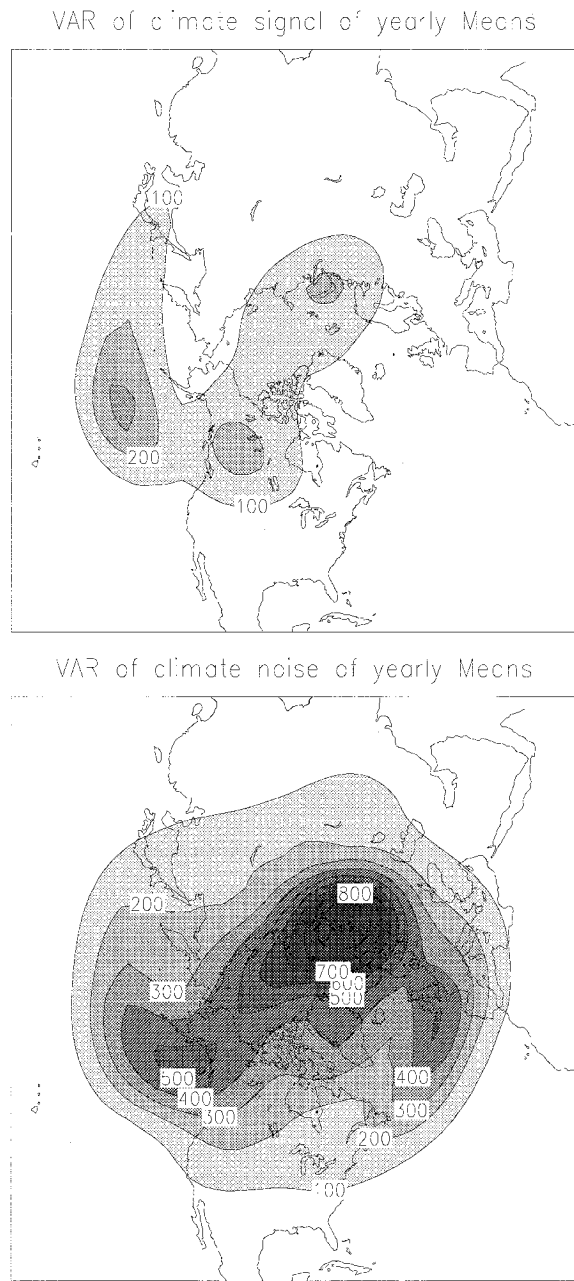


FIG. 3. Comparison of variance of yearly means between climate signal and noise (the contour unit is  $m^2$ ).

climate noise mainly develops over the Gulf of Alaska area, in between the two climate signal centers.

The variances of the decadal-mean climate signal and noise are shown in Fig. 4 (also in units of  $m^2$ ). The decadal variance is about an order of magnitude smaller than the yearly variance. The pattern of the noise variance is similar to that of the yearly means. However, the signal pattern is somewhat different. The decadal signal develops mainly over the western North Pacific and the adjacent Asian continent. Locally, the signal to noise ratio is better than 1. A slight amount of signal

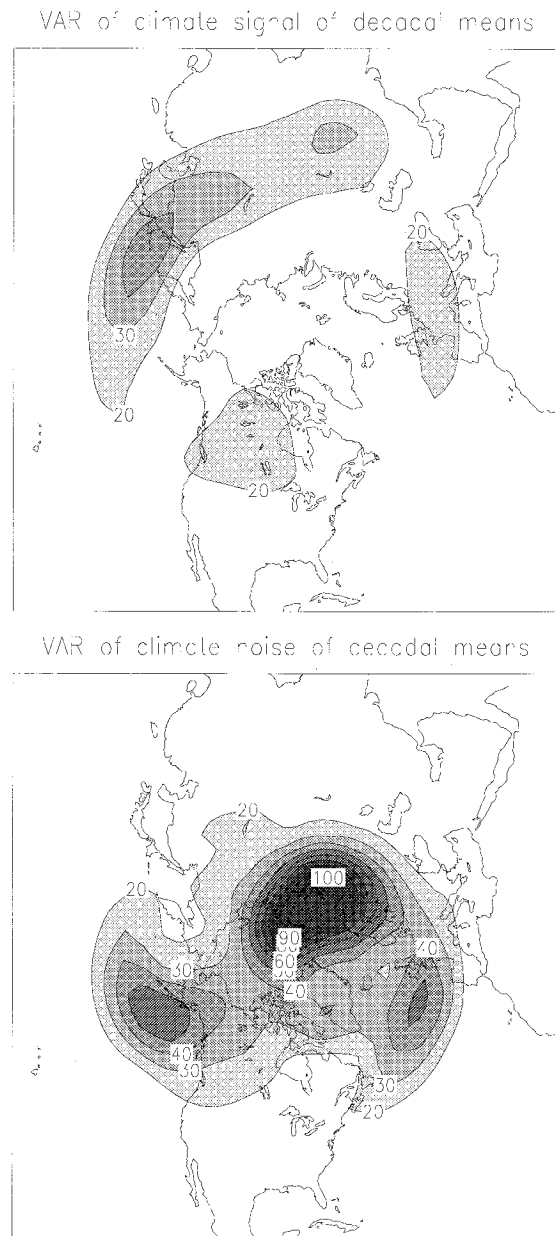


FIG. 4. As in Fig. 3 except for the decadal means.

variance can also be found over Europe. Again, much larger noise to signal ratio is observed over the AEA sector, explaining the significantly lower APC for AEA than PNA sector, as shown in Fig. 2.

The magnitude and patterns of the seasonal-mean climate signal and noise variance will be shown and discussed in the following sections.

### 5. Predictability due to El Niño versus La Niña type of forcing

Our experience and other recent studies (e.g., Kumar et al. 1996; Barnett 1995) suggest that the boundary

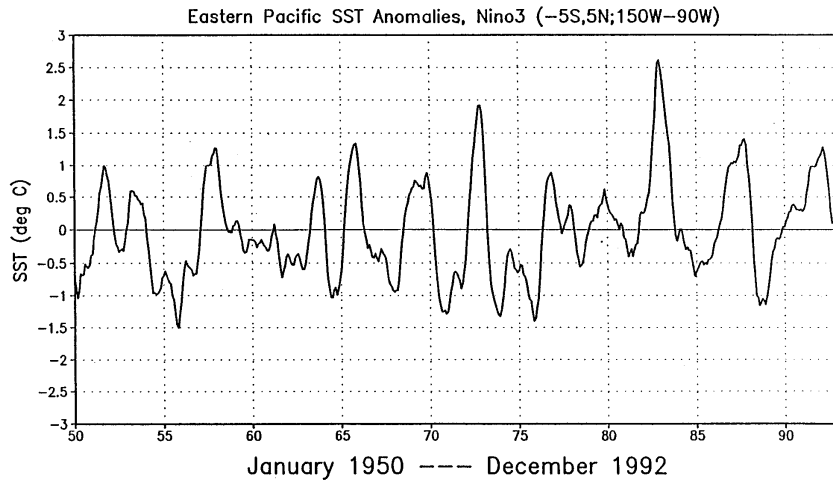


FIG. 5. Sea surface temperature time series over Niño-3. A low-pass temporal filter of 5-month running mean has been applied to the monthly mean data.

condition dependent predictability over the North Pacific is higher during the El Niño phase of the ENSO cycle than during the La Niña phase. The BCD predictability is not expected to be a simple linear response of the atmospheric time-mean flow to the tropical SST

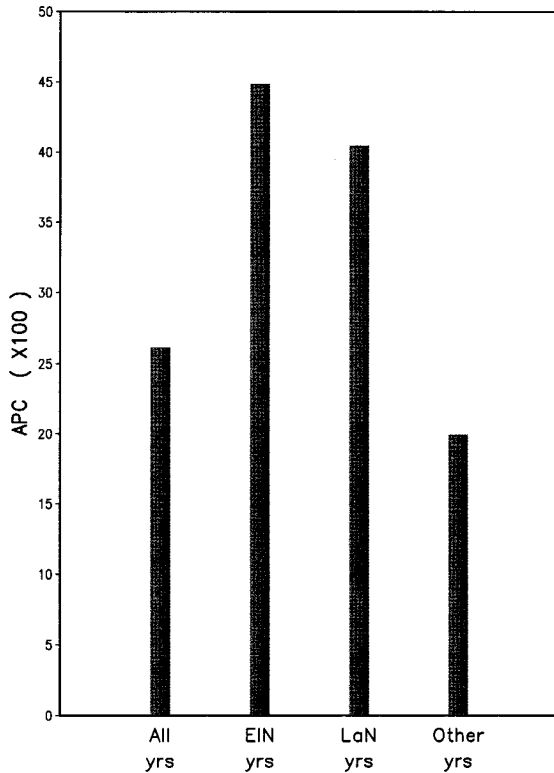


FIG. 6. Comparison of the stratified yearly mean predictability over the PNA sector. Result for all 44 years is denoted by “all yrs,” for the 6 El Niño/La Niña years by “EIN yrs/LaN yrs,” and for the 32 ENSO inactive years by “other yrs.”

anomalies. The present 13 45-yr GCM simulations should be able to bring this aspect into sharper focus.

The NCEP’s sea surface temperature reanalysis for the period from 1950 to 1992 (T. M. Smith et al. 1997, manuscript submitted to *J. Climate*) was used to construct the SST anomalies for the eastern tropical Pacific area. Niño-3, which covers the domain of 5°S–5°N and 150°W–90°W, was chosen to indicate the phase of the ENSO variation. Niño-3 SST anomalies from 1950 to 1992 are shown in Fig. 5. Based on this SST time series, El Niño and La Niña years can be identified. There were 6 El Niño and 6 La Niña events with the DJF seasonal-mean SST anomaly exceeding 1°C. Labelling the year (from August to next July) by January, the El Niño years are 1958, 1966, 1973, 1983, 1987, and 1992. The La Niña years are 1956, 1965, 1971, 1974, 1976, and 1989.

Figure 6 presents the stratified BCD predictability for the yearly means for 6 El Niño, 6 La Niña, and 32 other ENSO inactive years, for the PNA sector only. It is clear that the yearly mean predictability of the El Niño years is well above the average of those of the ENSO inactive years, 0.45 versus 0.20. The predictability for the La Niña years is similarly much higher but smaller than that of the El Niño years. The means and standard deviations and those of the Z-transformed statistics are listed in Table 3. The difference in APC between El

TABLE 3. Mean (M) and standard deviation (SD) of APCs before and after Fisher’s Z transformation for yearly climate means over the PNA sector.

| Time-scale | Z transformation | El Niño years |      | La Niña years |      | ENSO inactive years |      |
|------------|------------------|---------------|------|---------------|------|---------------------|------|
|            |                  | M             | SD   | M             | SD   | M                   | SD   |
| Yearly     | Before           | 0.45          | 0.33 | 0.40          | 0.28 | 0.20                | 0.33 |
|            | After            | 0.56          | 0.46 | 0.48          | 0.36 | 0.23                | 0.38 |

Niño and La Niña years, 0.45 versus 0.40, is small. However, the critical  $z$  score value, based on Eq. (6), regarding this difference turns out to be 2.96. At this level, it assures us that the difference is statistically significant with 99.5% confidence. We are now sure that over the PNA sector the BCD predictability is significantly higher during the El Niño years than the La Niña years, and both are much higher in predictability than the ENSO inactive years.

The variances of the yearly mean climate signal and noise are contrasted in Fig. 7 between the El Niño and La Niña years. The left-hand panels are for the climate signal, while the right-hand panels show the climate noise (the contour unit is  $m^2$ ). Over the North Pacific, the variance of climate signal during the El Niño phase is at least three times larger than during the La Niña phase, and about 10 times larger than during the ENSO inactive period of times. The variance of the climate noise is observed to be on the same order of magnitude for all three phases.

Comparison of the seasonal-mean predictability is next shown in Fig. 8, again for the PNA sector only. Large seasonality in predictability is immediately clear. During the warm phase of the ENSO cycle (top panel), the predictability is substantially above the average (the open circles) from early winter to late spring, reaching a maximum in January–March. During the cool phase of the ENSO cycle (middle panel), the predictability is higher than the average from the second half of the summer to the early winter, but the predictability drops rapidly to near average in spring. While the El Niño phase yields a high predictability in the spring, the La Niña phase encounters what might be called a spring barrier in predictability. A spring barrier has been reported for the SST predictions in the Tropics (Cane 1991; Latif and Graham 1991) and for the predictability of other tropical variables (e.g., Webster and Yang 1992). To our knowledge, there is no report available regarding an extratropical atmospheric predictability barrier. The atmospheric predictability barrier in spring appears to be a distinct characteristic for the La Niña episodes, not at all for the El Niño phases of the ENSO cycle. For ENSO inactive periods the seasonal-mean predictability is below average throughout the year (bottom panel).

## 6. Spring barrier in atmospheric predictability

The rapid drop in predictability for the La Niña episodes in springtime can be traced back to the climate signal and noise characteristics of this model's climate variability, as shown in Figs. 9 and 10. The evolution in climate signal (Fig. 9; in units of  $m$ ), as defined by (7) and averaged over six events, indicates 1) much larger magnitude and 2) much more persistence into the springtime for the El Niño years than the La Niña years. The evolution of the climate noise variance (Fig. 10; in units of  $dm^2$ ), as defined by (9) and averaged over six

events, indicates that more climate noise occurs in the spring for the La Niña years than the El Niño years. While the climate signal gives rise to predictability, the climate noise degrades it. The relative magnitude of climate signal and noise, as shown in Figs. 9 and 10, helps explain why the predictability remains at a high level in the springtime for El Niño events, while a spring barrier in predictability is encountered for the La Niña episodes.

The evolution of the northern extratropical climate signal can, in turn, be traced back to the forcing of the SST anomalies in the tropical Pacific, as shown in Fig. 11. In general, the El Niño years (left panels) start to increase their positive anomalies in May, reaching a maximum in December before they decrease gradually to an insignificant amount of positive SST anomaly in June. In contrast, the La Niña years (right panels) attain a larger magnitude of negative anomalies early in May and June, but relatively smaller negative SST anomalies thereafter; the negative SST anomaly rapidly diminishes to an insignificant amount right after reaching a maximum in December.

The spring barrier in the extratropical atmospheric predictability can therefore partially be associated with the inherently weak tropical SST forcing conditions for the La Niña phases of the ENSO cycle in the boreal springtime. Many improvements in tropical SST prediction have been reported in the last few years, and the spring barrier has largely been reduced (D. Chen 1995, personal communication). Based on the present result, however, the extratropical atmospheric BCD predictability will still encounter a spring barrier during the La Niña years when the tropical Pacific negative SST anomalies, in general, decrease in strength in the spring, as shown in the right-hand panels of Fig. 11. Even when the weak negative SST anomalies are well forecast by the ocean model (implying no barrier in the SST predictability), a spring barrier in the extratropical atmospheric predictability will still be present because of the weak tropical SST forcing conditions and high levels of climate noise cited above.

## 7. Reduction of climate noise by ensemble averaging

The relative magnitude of climate signal and noise shown in Figs. 3 and 4, as well as those in Figs. 7, 9, and 10, facilitate in explaining why the boundary-condition-dependent predictability can be raised if the climate noise is reduced. There are a few ways to reduce the climate noise: besides temporal smoothing (as those shown previously that the yearly mean predictability is larger than the seasonal-mean predictability) another readily available technique is to average a few realizations to form a new prediction, the ensemble forecasting approach (Kumar et al. 1996; Barnett 1995). Figure 12 presents another example showing higher predictability due to ensemble mean prediction. For this illustration,

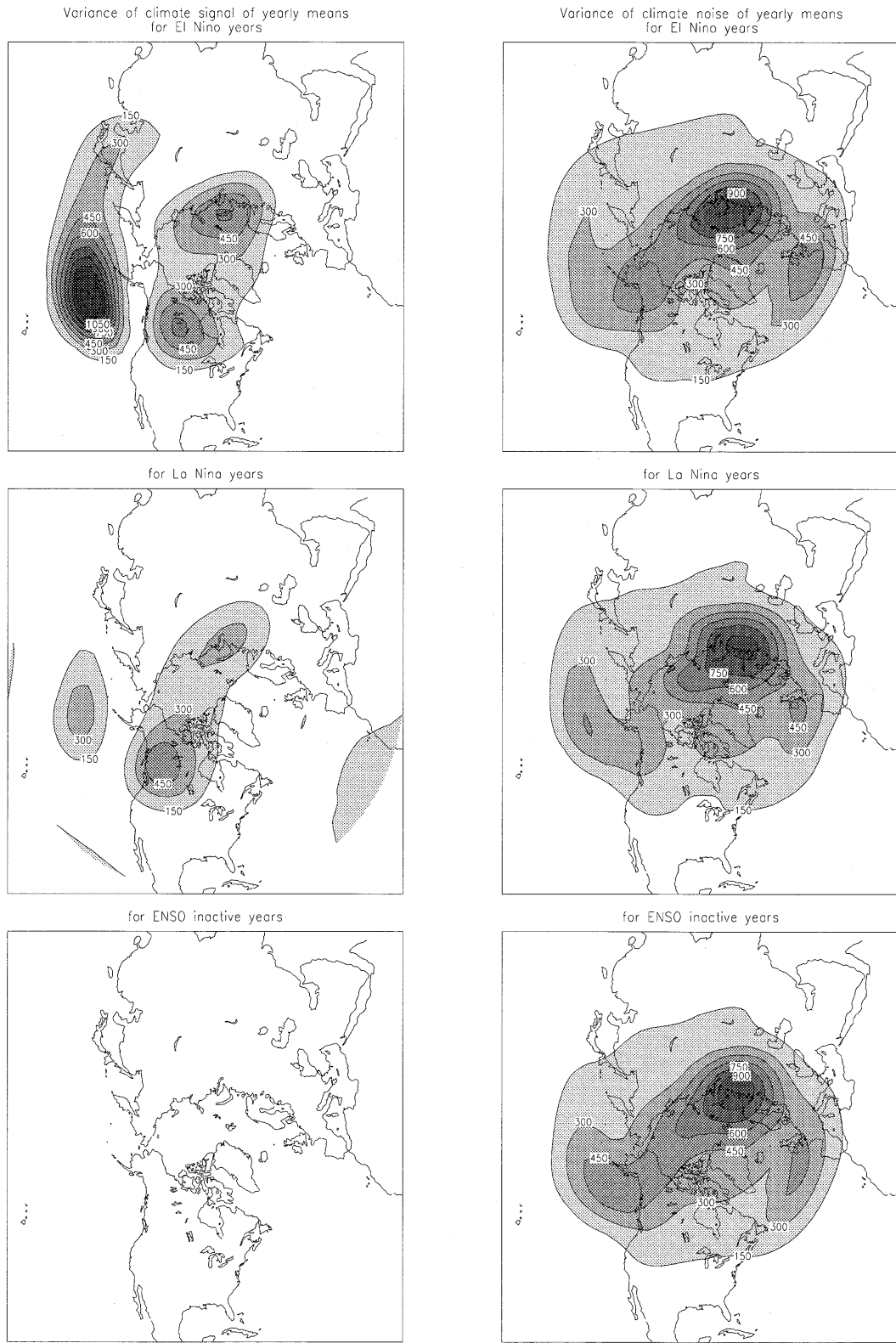


FIG. 7. Comparison of variance of yearly means between climate signal (left panels) and climate noise (right panels) for El Niño, La Niña, and ENSO inactive years (the contour unit is  $m^2$ ).

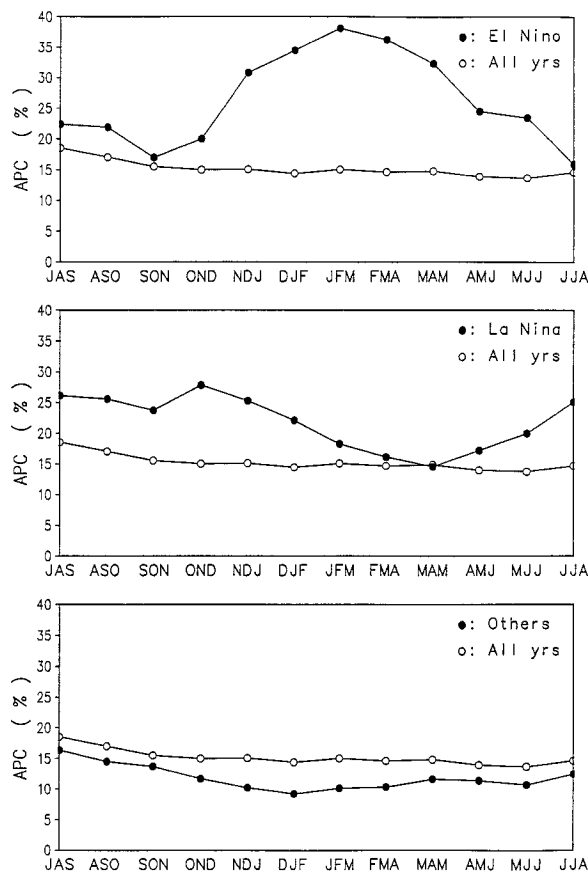


FIG. 8. Seasonality of the predictability of seasonal means over the PNA sector. Note that the predictability level is quite different between El Niño and La Niña years, especially in springtime.

we form a yearly mean ensemble prediction by averaging 12 out of the 13 total runs and saving the unused run as the realization to be verified against. (Since the real atmospheric state can not occur more than once, we ought to use only one run to represent it, although the simulated observation could be formed by more than one run.) Altogether 13 prediction–verification pairs can be constructed for each year, versus 78 twin experiments realized earlier. The statistical reliability of the estimated predictability is no longer as stable as the earlier ones, as shown in Fig. 6. But when comparing Fig. 12 to Fig. 6, it is clear that the climate noise of an ensemble-mean prediction can be reduced and the theoretical predictability can be raised, as has been reported by Kumar et al. (1996) and Barnett (1995). Taking the El Niño years, for instance, the predictability level is now 0.63 versus 0.45 found in Fig. 6, a gain of nearly 20 points through the employment of the ensemble-mean operator.

The seasonality in predictability has been seen in Fig. 8 to be widely different between El Niño and La Niña type of forcing conditions. It should be interesting to see whether or not the ensemble mean prediction still shows the same seasonality behavior. Figure 13 presents the results. For this case the ensemble mean was also formed

by 12 runs and there were 13 prediction–verification pairs for each season. Besides yielding higher predictability values for the ensemble-mean predictions, the relative magnitude among those three groups shown in Fig. 13 is much the same as in Fig. 8. The ensemble predictability for the El Niño type of forcing conditions is higher in springtime, while it is much lower for the La Niña-type of forcing conditions and below the average predictability level for those ENSO inactive seasons.

### 8. Implication in short-term climate prediction

From Figs. 12 and 13 we may extrapolate that, even if the climate noise can be reduced to a minimum and the climate signal isolated to its full extent owing to sufficient computational power, we still have to face the fact that the boundary condition dependent predictability has an upper limit. This is simply because the verification field, be it a model or real atmosphere, always contains a huge amount of climate noise.

The problem in application of an atmospheric general circulation model to short-term climate prediction appears to be reduced to 1) How good is the atmospheric model’s climatology? 2) How close to reality is the magnitude of the model variability? 3) How similar are the climatic-scale model teleconnection patterns to those observed? The following figures offer some insights into the above questions.

Figure 14 compares the Z500 climatology and variability between the model (MDL) and the observed (OBS) for the winter season. The climatologies, after the zonal mean is removed to focus on the stationary waves (the upper panels), show grossly similar patterns except for the Siberia region. The lower panels compare the interannual variability of the seasonal means (the contour unit is  $\text{dam}^2$ ). Now we find a serious discrepancy between the MDL and the OBS: much smaller variability for the model runs. Taking the North Pacific center of variance, for instance, it is about 60 versus 45  $\text{dam}^2$  and the MDL variance is shifted downstream, as described earlier by Chen and Van den Dool (1995b). The interannual variance of the model atmosphere is only about 75% of the real atmosphere except over Novaya Zemlya where the model has an odd maximum.

Perhaps a couple of specific examples would help in gaining some insights into the current model deficiencies described above. For El Niño DJF (1986/87) and La Niña DJF (1988/89) observations, predictions and validation are shown in Figs. 15 and 16. The observed Z500 anomalies are displayed in the top left panel, the ensemble averaged climate signals in the top right panel, the individual and ensemble APC forecast skill in the bottom right panel, where the solid bar stands for the ensemble forecast skill and the dashed horizontal line the average of the 13 APCs. The model anomalies of each individual run are labeled as GCM runs 1–13 in the figure.

From so much information in the figures, we simply would like to point out a few features.

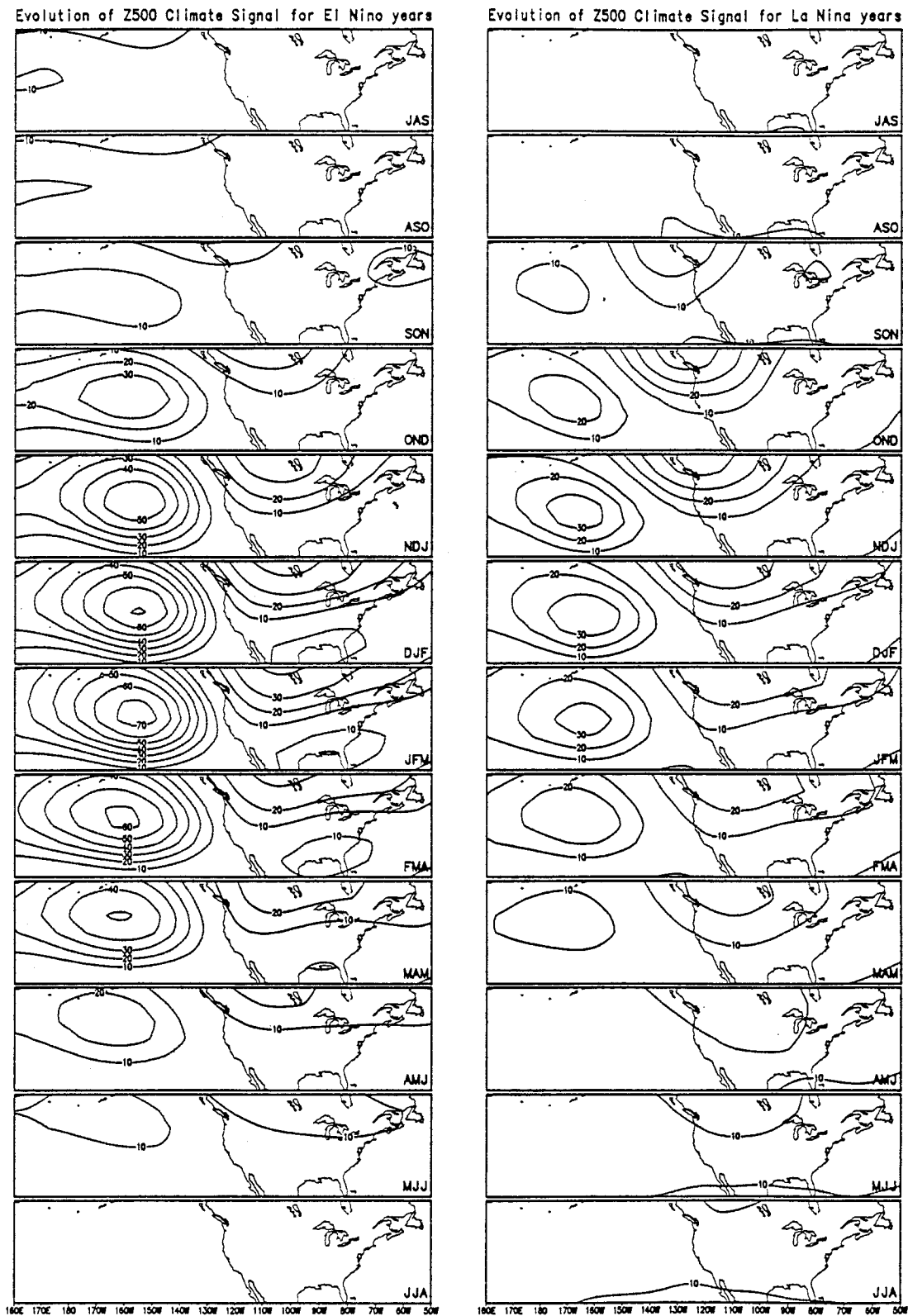


FIG. 9. Comparison of climate signal evolution between the El Niño years (left panels) and the La Niña years (right panels) (the seasonal mean contour unit is m).

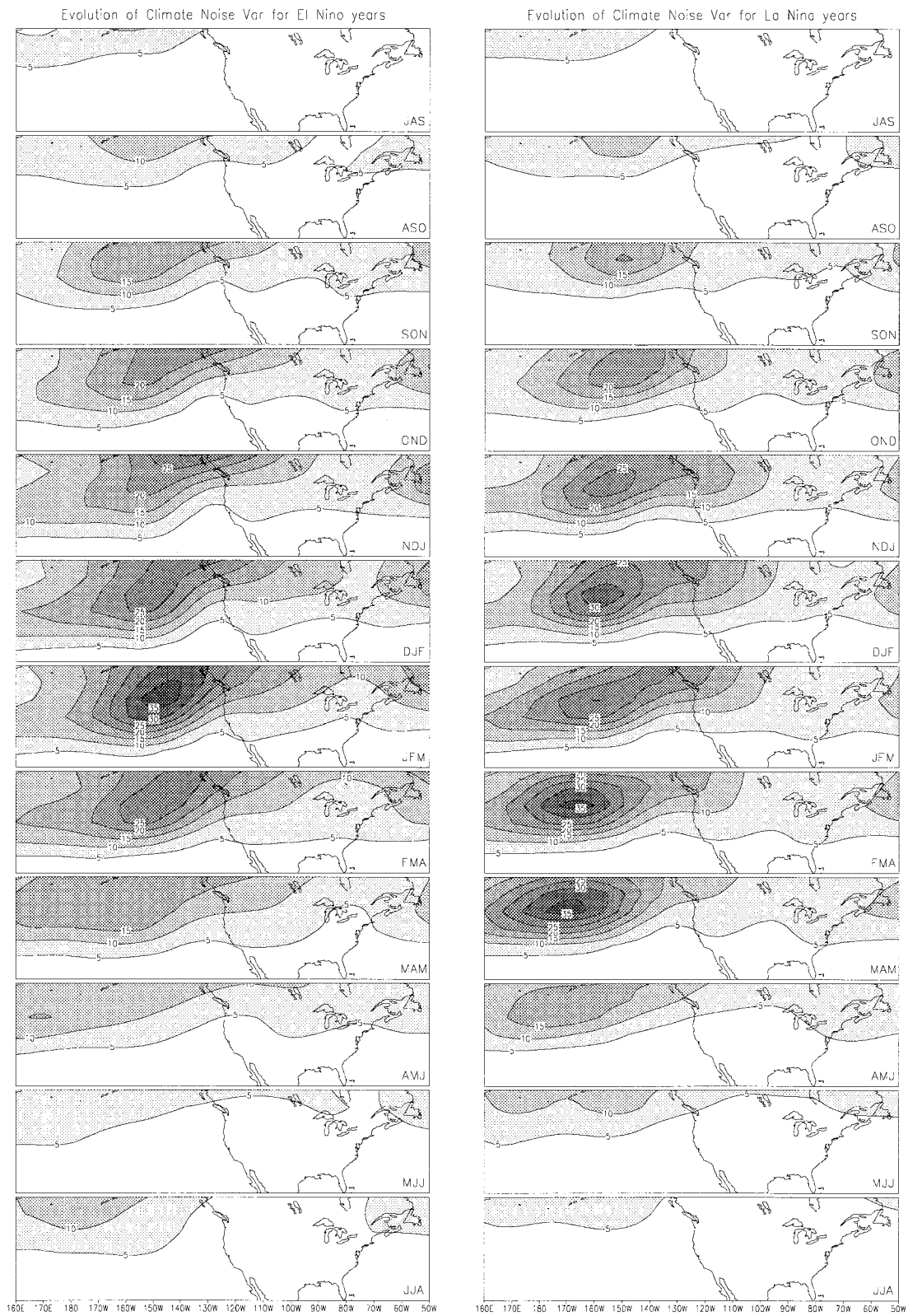


FIG. 10. As in Fig. 9 except for the climate noise variance (the contour unit is now  $\text{dam}^2$ ).

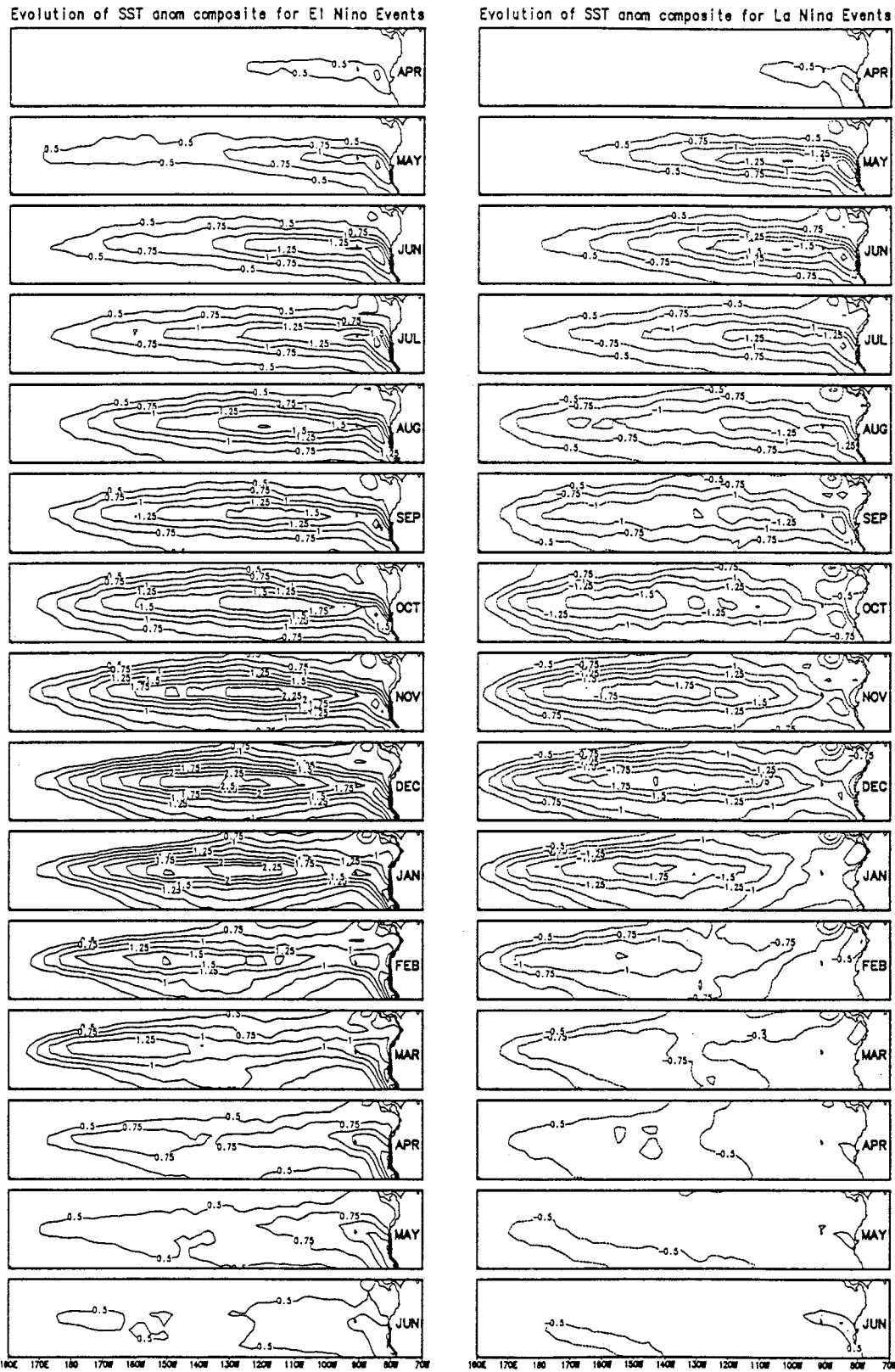


FIG. 11. As in Figs. 9 and 10 except for the tropical Pacific SST anomaly composites for the monthly means (the contour unit is  $^{\circ}\text{C}$ ).

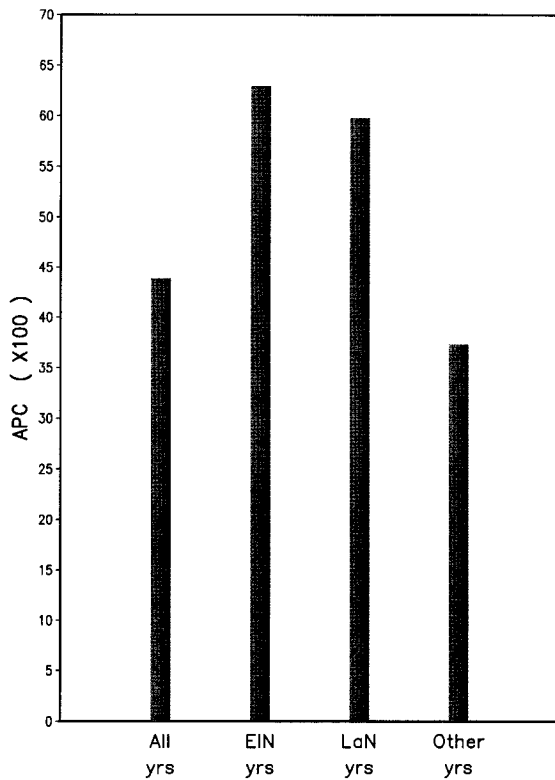


FIG. 12. As in Fig. 6 except for ensemble-mean predictability. The ensemble means were constructed from 12 runs. Details can be found in section 7. Note that the level of predictability is about 20 points higher than those in Fig. 6.

- 1) The model anomalies are very noisy from case to case in both magnitude and location, implying a huge amount of model climate noise. Careful inspection will show that those in Fig. 16 (La Niña DJF) are noisier than those in Fig. 15 (El Niño DJF).
- 2) In general, the model anomalies are too weak relative to the OBS. In Fig. 15, only runs 2 and 9 out of 13 have comparable negative anomaly in the North Pacific; only runs 7, 9, 10, and 13 out of 13 have comparable positive anomaly over North America. Similar weaknesses in the model anomalies can also be detected in Fig. 16. The weakness in model anomalies is consistent with earlier observations that the MDL variability is much weaker than the observed (Fig. 14), a major model deficiency indeed.
- 3) The climate signals (top right panels) are rather small in magnitude, to the extent that not all of the teleconnection anomaly centers are present as observed (top left panels), although we have to recognize that the OBS anomalies represent only one possible realization of the atmospheric states and contain therefore a large amount of climate noise. However, we have repeatedly observed recognizable PNA or TNH (Barnston and Livezey 1987) multicentered teleconnection patterns in the real atmosphere during both warm and cold phases of the ENSO cycle. Therefore, lack of a multicentered teleconnection pattern in the

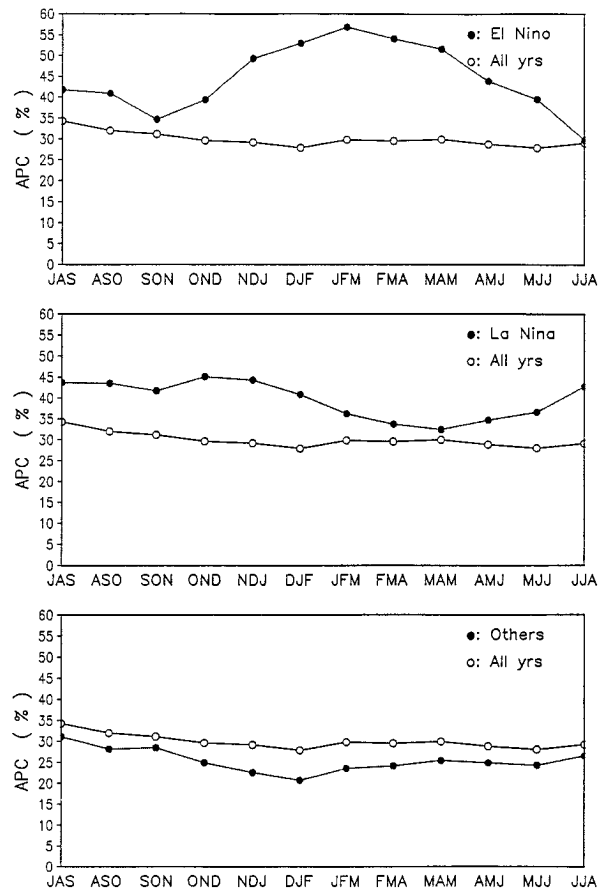


FIG. 13. As in Fig. 8 except for ensemble-mean predictability. Note that the level of predictability is about 20 points higher than those in Fig. 8.

- ensemble forecast constitutes another major model deficiency. This, in a way, is closely related to the deficiency mentioned above in 2).
- 4) The bottom right panels show, on average, that there is skill in the model forecasts. The ensemble forecast is much better than the average of the individual forecast. Finally, the El Niño ensemble forecast is much better than the La Niña forecast, as expected.

From the above specific cases and the comparisons of the interannual variance as shown in Fig. 14, a major deficiency of the current atmospheric model appears to be the inability of the model to generate climate anomalies with sufficient magnitude. The implication is that an extreme climate event will likely be underestimated by an individual GCM run and, almost for sure, cannot be expected from an ensemble average prediction. How to enhance the model climate variability appears to be an important task in the continuing effort of improving the atmospheric model performance.

**9. Summary and conclusions**

The variability and predictability of climate means for the northern extratropical atmosphere are examined.

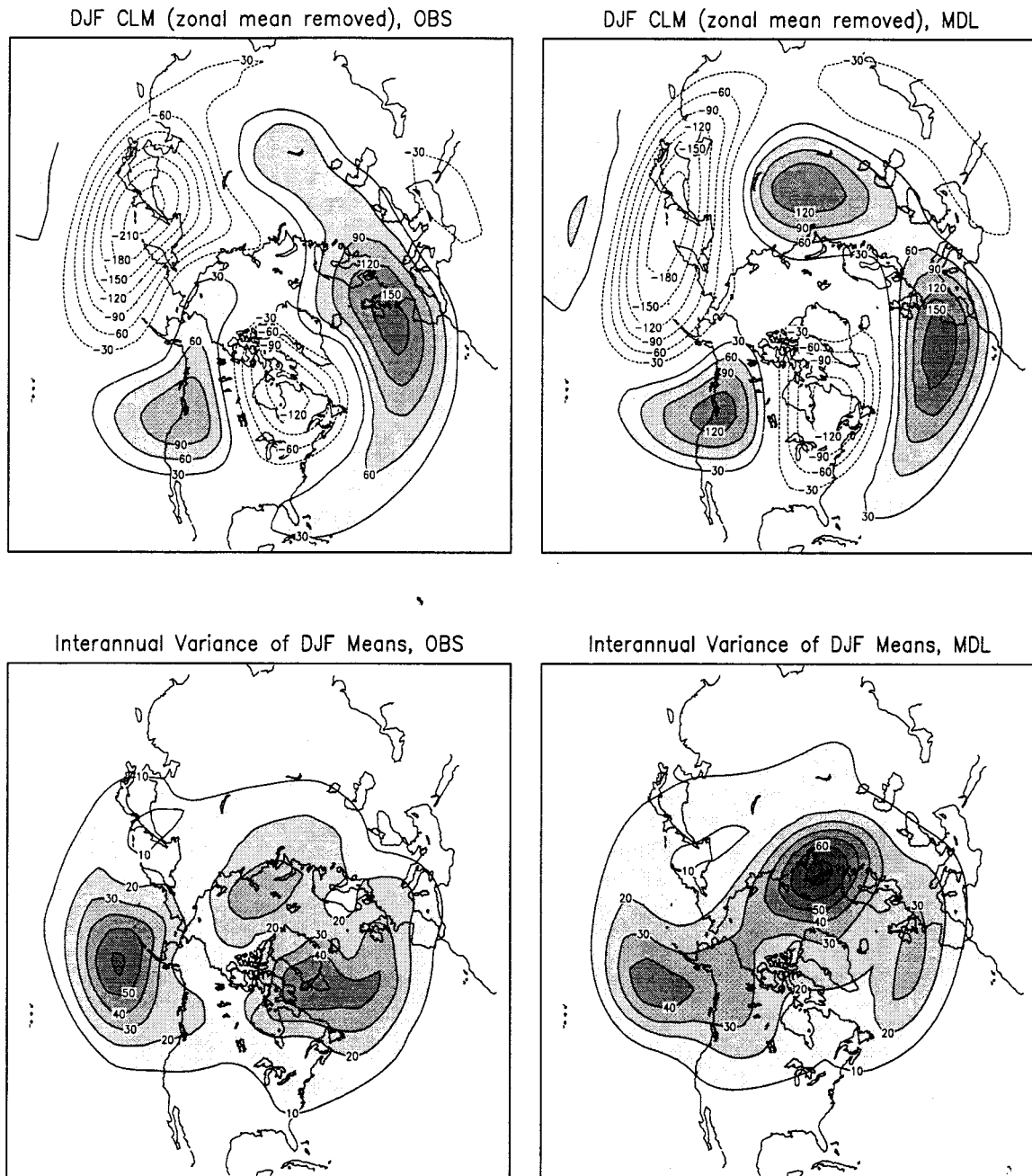


FIG. 14. Upper panels: comparison of the Z500 DJF climatologies (with the zonal mean removed) between the model results and those observed. Contour unit is gpm. The positive deviations from zonal mean are shaded for better contrast. Lower panels: comparison of the interannual variance between the model results and those observed the contour unit is  $\text{dam}^2$ .

The emphasis and approach of this article deviates from the classic predictability studies. While the classic study focuses on the sensitive dependence on the initial conditions, our emphasis is on the dependence of the predictability on the boundary forcing conditions. The classic predictability examines the error growth rate and the limit of deterministic predictability; the present study investigates the climate signal and noise contained in the climate variability and determines how dependent

they are upon the external boundary conditions. The study of externally forced potential predictability is not new. In fact, it has been extensively explored in recent decades by various groups and individuals, such as listed in the introduction and the references. While most of the previous studies conducted comparisons between the simulated variability and the observed, we narrow our focus to a perfect model point of view. Without reference to the real atmospheric states, we tried to determine

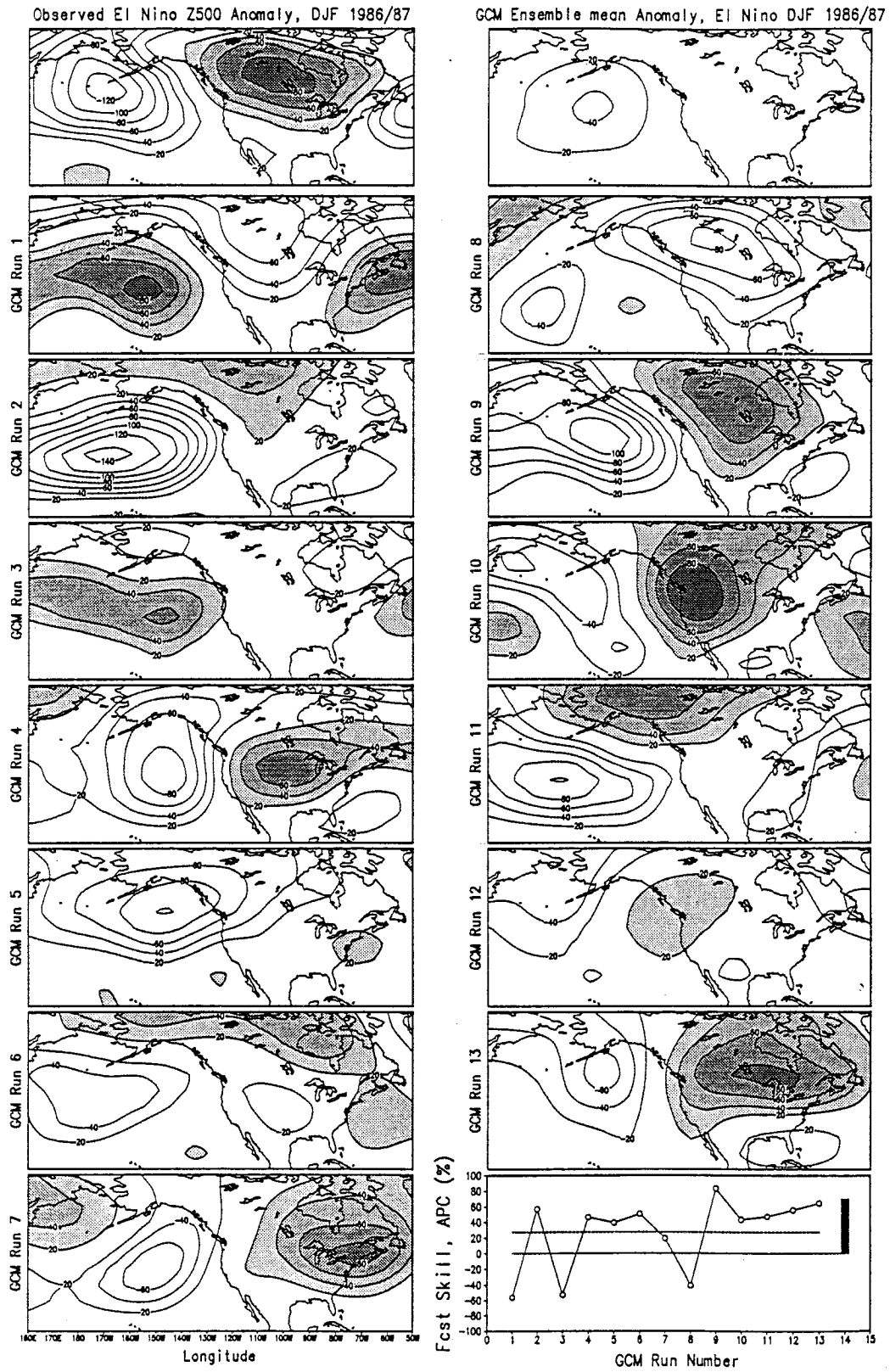


FIG. 15. Top left: observed anomalies for El Niño DJF (1986/87). Top right: the corresponding GCM 13-run ensemble-averaged climate signals. Bottom right: the individual and ensemble-mean (solid bar) APC forecast skill scores. The dashed horizontal line is the average of the 13 individual APCs. The rest: the model anomalies for each individual run.

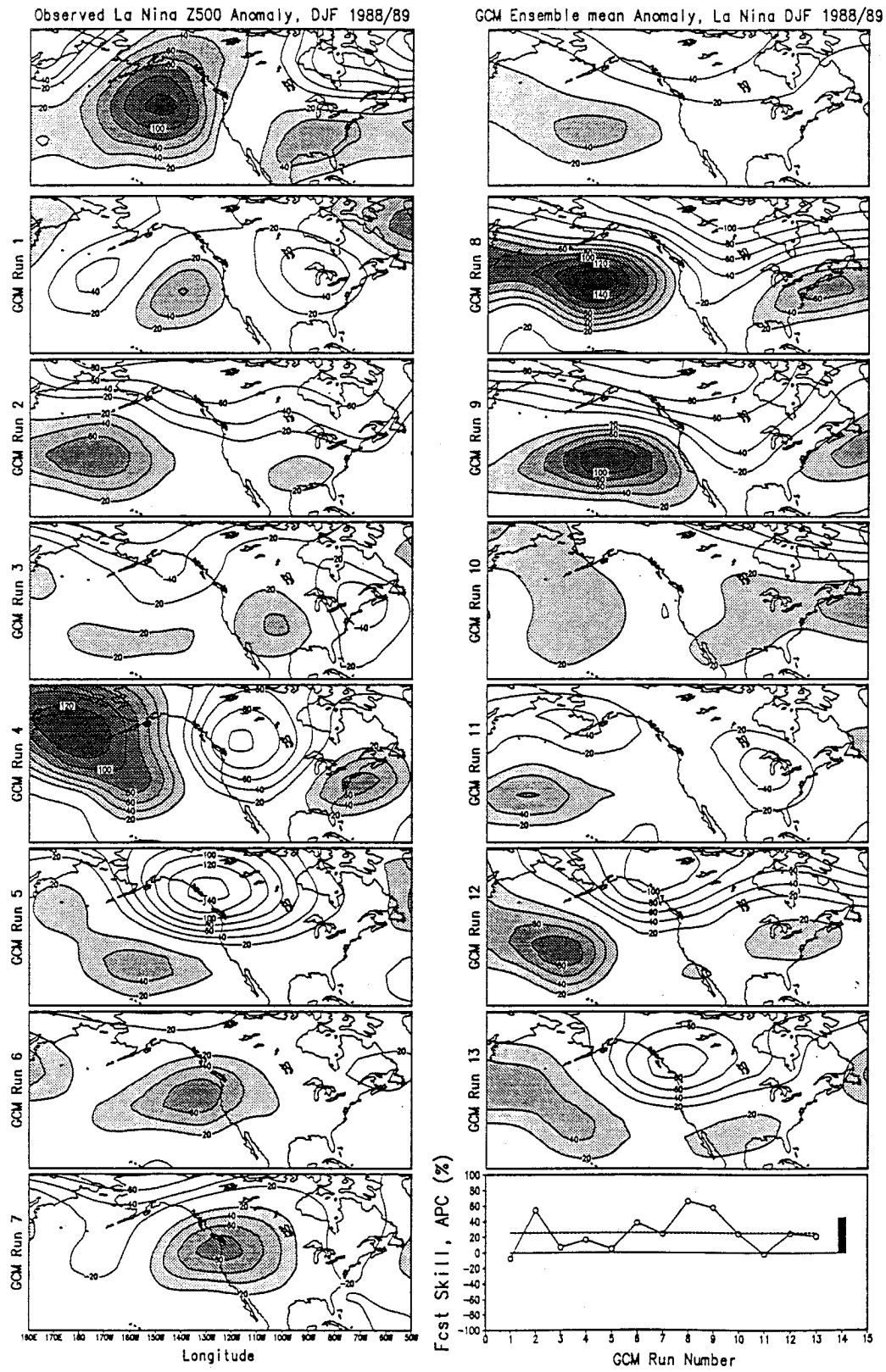


FIG. 16. As in Fig. 15 except for La Niña DJF (1988/89).

the theoretical upper bound of the atmospheric predictability that is boundary condition dependent.

A large climate variability experiment conducted by the Coupled Model Project of the National Centers for Environmental Prediction was analyzed. The boundary-condition-dependent predictability at seasonal to decadal timescales is evaluated. Major limitations and deficiencies of the current atmospheric model for the purpose of short-term climate prediction are also examined.

The decadal-mean predictability is found to be less than 0.40 in APC skill score for the Northern Hemisphere domain ( $20^{\circ}$ – $70^{\circ}$ N). The predictability decreases to 0.22 for the yearly means and to less than 0.15 for the seasonal means. When examined separately for different regions, the BCD predictability over the PNA sector ( $120^{\circ}$ E– $60^{\circ}$ W) is found to be significantly larger than over the AEA sector ( $60^{\circ}$ W– $120^{\circ}$ E): 0.26 versus 0.18 for the yearly means and 0.45 versus 0.34 for the decadal means. The differences in the mean predictability cited above are statistically significant with near 100% confidence. The above results imply that there is a larger or better detectable impact from the tropical Pacific SST anomaly forcing on the predictability over the PNA sector than the AEA sector.

The geographical distribution of the interannual variability of climate signal and climate noise shows larger signal variance over the PNA sector than the AEA sector, while the noise variance shows much smaller magnitude over the PNA than the AEA sector. This large difference in signal to noise ratio results in much larger APC score (cf. Van den Dool and Toth 1991) for the PNA sector than the AEA sector.

When the predictability is evaluated separately for the El Niño, La Niña, and ENSO inactive periods of time, then a large difference in impact of the ENSO SST anomalous forcing on the predictability over the PNA sector can be observed. The El Niño phase of the ENSO cycle yields much higher predictability than the 44-year average, while the ENSO inactive phase exhibits lower predictability than normal. The La Niña years also yield significantly higher predictability than normal, but it is significantly smaller than those of the El Niño years. Taking the yearly mean predictability for example, the APC score is 0.45 for the El Niño years and 0.40 for the La Niña years versus 0.20 for the ENSO inactive years. The reason for the large difference can be found in the magnitude of the climate signal generated by the tropical SST anomalous forcing. The noise variance is to the same order of magnitude for all three phases of the ENSO cycle. These results are consistent with those reported by Kumar et al. (1996) and Barnett (1995).

For seasonal means, a substantial seasonality in predictability is observed. In warm ENSO years, the BCD predictability increases way above the average from early winter to late spring. In contrast, the predictability drops rapidly to near average in spring for the cold ENSO episodes. The spring barrier in atmospheric predictability appears to be a phenomenon for the La Niña

type forcing conditions only. The cause of the predictability barrier in spring can be traced back to the inherently weak tropical SST forcing conditions in the springtime for the La Niña years of the ENSO cycle and the higher noise level.

In this paper the predictability is gauged by the APC scores and the closely related climate-signal to climate-noise ratio. There are other measures that could bring to light other aspects of the predictability issue not discussed here. For instance, using the full probability distribution function may bring to light changes in probability too subtle to be measured by the APC skill score.

Due to the nature of the large magnitude of climate noise in the climate interannual variability, the predictability of climate means will always have an upper bound, even for a perfect model atmosphere and even when a large ensemble mean prediction is exploited. This is because the verification field, in order to simulate the real atmospheric state that can never occur more than once, always contains a large amount of climate noise.

Three aspects regarding the application of an atmospheric general circulation model in short-term climate prediction were examined: 1) how good is the atmospheric model climatology, 2) how realistic is the model's low-frequency variability, and 3) how similar to the observed is the multicentered pattern of the teleconnectivity in the model climate variability.

The climatology of the current atmospheric model compares well with the observed. The interannual variability of the model climate shows, however, only about 75% of the real atmospheric variance, constituting a major deficiency in this model. Due to this weakness, nature's multicentered teleconnection pattern cannot be reproduced in a single member prediction, let alone in an ensemble average. A large climate event will likely be underestimated by an individual GCM run due to small chances that an individual run will attain large climate anomaly, and a multicentered teleconnection pattern may not be expected by an ensemble mean forecast. Therefore, how to enhance the model climate variability appears to be an urgent task in the continuing effort in improving the performance of this atmospheric general circulation model. The displacements of the variance centers (MDL vs OBS) are other model deficiencies to be improved upon.

*Acknowledgments.* The monthly mean output dataset of this large-scale experiment were kindly made available to us by Dr. Ming Ji. The authors would like to thank him and other colleagues in the ocean-atmosphere coupled model group at the National Centers for Environmental Prediction for their combined efforts and support, without which the present study would not have been possible. The authors would also like to thank Drs. A. Kumar, Jae Schemm, and D. Unger and two anonymous reviewers for their critical reviews of this article. Their comments and suggestions have much improved the contents of this article.

## REFERENCES

- Barnett, T. P., 1995: Monte Carlo climate forecasting. *J. Climate*, **8**, 1005–1022.
- Barnston, A. G., and R. E. Livezey, 1987: Classification, seasonality, and persistence of low-frequency atmospheric circulation patterns. *Mon. Wea. Rev.*, **115**, 1083–1126.
- Blackmon, M. L., J. E. Geisler, and E. J. Pitcher, 1983: A general circulation model study of January climate anomaly patterns associated with interannual variation of equatorial Pacific sea surface temperatures. *J. Atmos. Sci.*, **40**, 1410–1425.
- Blumenthal, M. B., 1991: Predictability of a coupled ocean–atmosphere model. *J. Climate*, **4**, 766–784.
- Branstator, G., 1986: The variability in skill of 72-hour global-scale NMC forecasts. *Mon. Wea. Rev.*, **114**, 2628–2639.
- Cane, M. A., 1991: Forecasting El Niño with a geographical model. *Teleconnections Connecting World-Wide Climate Anomalies*, M. Glantz, R. Katz, and N. Nicholls, Eds., Cambridge University Press, 345–369.
- Chen, W. Y., 1989: Estimate of dynamical predictability from NMC DERF experiments. *Mon. Wea. Rev.*, **117**, 1227–1236.
- , and H. M. Van den Dool, 1995a: Low frequency variabilities for widely different basic flows. *Tellus*, **47A**, 526–540.
- , and —, 1995b: Low-frequency anomalies in the NMC MRF model and reality. *J. Climate*, **8**, 1369–1385.
- Chervin, R. M., 1986: Interannual variability and seasonal climate predictability. *J. Atmos. Sci.*, **43**, 233–251.
- Cubash, U., 1985: The mean response of the ECMWF global model to the composite El Niño anomaly in the extended range prediction experiments. *Coupled Ocean–Atmosphere Models*, J. Nihoul, Ed., Elsevier Press, 329–344.
- Dalcher, A., and E. Kalnay, 1987: Error growth and predictability in operational ECMWF forecasts. *Tellus*, **39A**, 474–491.
- Folland, C. K., and D. P. Rowell, 1995: Workshop on Simulations of the Climate of the Twentieth Century Using GISST. Climate Research Tech. Rep. 56, 111 pp.
- Fraedrich, K., 1988: El Niño/Southern Oscillation predictability. *Mon. Wea. Rev.*, **116**, 1001–1012.
- Goswami, B. N., and J. Shukla, 1991: Predictability of a coupled ocean–atmosphere model. *J. Climate*, **4**, 3–22.
- Horel, J. D., and J. M. Wallace, 1981: Planetary scale atmospheric phenomena associated with the Southern Oscillation. *Mon. Wea. Rev.*, **109**, 813–829.
- Hoskins, B. J., and D. J. Karoly, 1981: The steady linear response of a spherical atmosphere to thermal and orographic forcing. *J. Atmos. Sci.*, **38**, 1179–1196.
- Jones, R. H., 1975: Estimating the variance of time averages. *J. Appl. Meteor.*, **14**, 159–163.
- Kalnay, E., M. Kanamitsu, and W. E. Baker, 1990: The NMC global forecast system. *Bull. Amer. Meteor. Soc.*, **71**, 1410–1428.
- Kanamitsu, M., 1989: Description of the NMC Global Data Assimilation and Forecast System. *Wea. Forecasting*, **4**, 335–342.
- Kumar, A., M. Hoerling, M. Ji, A. Leetmaa, and P. Sardeshmukh, 1996: Assessing a GCM’s suitability for making seasonal predictions. *J. Climate*, **9**, 115–129.
- Latif, M., and N. E. Graham, 1991: How much predictive skill is contained in the thermal structure of an OGCM? *TOGA Notes*, **2**, 6–8.
- Lau, N. C., 1981: A diagnostics study of recurrent meteorological anomalies appearing in a 15-year simulation with a GFDL general circulation model. *Mon. Wea. Rev.*, **109**, 2287–2311.
- Leith, C. E., 1973: The standard error of time-average estimates of climatic means. *J. Appl. Meteor.*, **12**, 1066–1069.
- Lorenz, E. N., 1965: A study of the predictability of a 28-variable atmospheric model. *Tellus*, **17**, 321–333.
- , 1982: Atmospheric predictability experiments with a large numerical model. *Tellus*, **34**, 505–513.
- Madden, R. A., 1976: Estimates of the natural variability of time-averaged sea-level pressure. *Mon. Wea. Rev.*, **104**, 942–952.
- Mansfield, D. A., 1986: The skill of dynamical long-range forecasts, including the effect of sea surface temperature anomalies. *Quart. J. Roy. Meteor. Soc.*, **112**, 1145–1176.
- Miyakoda, K., G. D. Hembree, R. F. Stricker, and I. Shulman, 1972: Cumulative results of extended forecast experiments: I. Model performance for winter cases. *Mon. Wea. Rev.*, **100**, 836–855.
- , J. Sirutis, and J. Ploshay, 1986: One-month forecast experiments—Without anomaly boundary forcings. *Mon. Wea. Rev.*, **114**, 2363–2401.
- Morrison, D. F., 1983: *Applied Linear Statistical Methods*. Prentice-Hall, 562 pp.
- Palmer, T. N., and S. Tibaldi, 1988: On the prediction of forecast skill. *Mon. Wea. Rev.*, **116**, 2453–2480.
- Rasmusson, E. M., and J. M. Wallace, 1983: Meteorological aspects of the El Niño/Southern Oscillation. *Science*, **222**, 1195–1202.
- Roads, J. O., 1986: Forecasts of time averages with a numerical weather prediction model. *J. Atmos. Sci.*, **43**, 871–892.
- , 1987: Predictability in the extended range. *J. Atmos. Sci.*, **44**, 3405–3527.
- Rowell, D. P., C. K. Folland, K. Maskell, and M. N. Ward, 1995: Variability of summer rainfall over tropical North Africa (1906–92): Observations and modelling. *Quart. J. Roy. Meteor. Soc.*, **121**, 669–704.
- Saha, S., and H. M. Van den Dool, 1988: A measure of the practical limit of predictability. *Mon. Wea. Rev.*, **116**, 2522–2526.
- Scheffe, H., 1959: *The Analysis of Variance*. John Wiley and Sons, 477 pp.
- Schubert, S. D., and M. Suarez, 1989: Dynamical predictability in a simple general circulation model: Average error growth. *J. Atmos. Sci.*, **46**, 353–370.
- Sela, J. G., 1980: Spectral modeling at the National Meteorological Center. *Mon. Wea. Rev.*, **108**, 1279–1292.
- Shukla, J., 1981: Dynamical predictability of monthly means. *J. Atmos. Sci.*, **38**, 2547–2572.
- Smagorinsky, J., 1969: Problems and promises of deterministic extended range forecasting. *Bull. Amer. Meteor. Soc.*, **50**, 285–311.
- Tracton, M. S., K. Mo, W. Chen, E. Kalnay, R. Kistler, and G. White, 1989: Dynamical extended range forecasting (DERF) at the National Meteorological Center. *Mon. Wea. Rev.*, **117**, 1604–1635.
- Trenberth, K. E., 1984: Some effects of finite sample size and persistence on meteorological statistics. Part II: Potential predictability. *Mon. Wea. Rev.*, **112**, 2369–2379.
- Van den Dool, H. M., 1994: Long range weather forecasts through numerical and empirical methods. *Dyn. Atmos. Oceans*, **20**, 247–270.
- , and Z. Toth, 1991: Why do forecasts for “near-normal” often fail? *Wea. Forecasting*, **6**, 76–85.
- Wallace, J. M., and M. L. Blackmon, 1983: Observation of low-frequency atmospheric variability. *Large-Scale Dynamical Processes in the Atmosphere*, B. J. Hoskins and R. P. Pearce, Eds., Academic Press, 55–94.
- Webster, P. J., and S. Yang, 1992: Monsoon and ENSO: Selectively interactive systems. *Quart. J. Roy. Meteor. Soc.*, **118**, 877–926.
- Zwiers, F. W., 1987: A potential predictability study conducted with an atmospheric general circulation model. *Mon. Wea. Rev.*, **115**, 2957–2974.
- , 1996: Interannual variability and predictability in an ensemble of AMIP climate simulations conducted with the CCC GCM2. *Climate Dyn.*, **12**, 825–847.